JOURNAL OF AIRCRAFT
Vol. 46, No. 3, May–June 2009

Flow Measurements in a Short Takeoff, Vertical Landing Fountain: Splayed Jets

A. J. Saddington,* K. Knowles,† and P. M. Cabrita‡
Cranfield University, Shrivenham, Swindon SN6 8LA, United Kingdom

DOI: 10.2514/1.38296

The interaction of multiple jets with the ground is of great importance for the design and operation of short takeoff, vertical landing aircraft. The fountain upwash flow, generated by the impingement of two axisymmetric, compressible, turbulent jets onto a ground plane was studied using laser-based particle image velocimetry. Measurements were made with nozzle pressure ratios of between 1.05 and 4, nozzle height-to-diameter ratios of between 2.4 and 8.4, nozzle splay angles of between ±15 deg, and a nozzle spacing-to-diameter ratio of seven. The effect of varying these parameters on the fountain velocity decay, spreading rate, and momentum flux ratio are discussed. In general, it was found that the inclusion of nozzle splay did not significantly alter the distribution of fountain momentum flux ratio relative to the equivalent parallel configuration.

Nomenclature

a_1 = growth rate of the fountain half-width (see Eq. (4))
a_2 = fountain half-width at $z = 0$ (see Eq. (4))
D = nozzle exit internal diameter
H = nozzle exit height above the ground plane (see Fig. 1)
J = proportion of jet momentum carried downstream after impingement (i.e. downstream momentum divided by total jet momentum)
L = theoretical distance between the jets' stagnation points at impingement (see Fig. 1)
$\dot{M}$ = fountain momentum flux
$\dot{M}_{\max}$ = maximum fountain vertical momentum flux
r = radial distance from the nozzle axis
S = distance between the nozzle centers (see Fig. 1)
U = time–mean velocity in the streamwise direction
$\hat{U}$ = time–mean peak streamwise velocity in the fountain
U_j = time–mean jet centerline velocity at the nozzle exit
$U_{\max}$ = time–mean local maximum streamwise velocity in the fountain
u = instantaneous velocity in the streamwise direction (positive downwards for jets; positive upwards for fountain)
v = instantaneous velocity in the x-direction
x = coordinate parallel to the ground plane in the plane of the jet centers (see Fig. 1)
$x_{0.5}$ = fountain half-width where $U = U_{\max}/2$
x_1 = fountain width
y = coordinate parallel to the ground plane in the plane of the nominal fountain axis (see Fig. 1)
z = coordinate normal to the ground plane (see Fig. 1)
α = nozzle splay angle (positive outwards)
$\lambda_{\dot{M}}$ = fountain momentum flux ratio ($\dot{M}/\dot{M}_{\max}$)
ρ = air density
ϕ = jet spreading half-angle (see Fig. 1)

Received 28 April 2008; revision received 19 December 2008; accepted for publication 19 December 2008.

*Lecturer, Defence Academy of the United Kingdom, Aeromechanical Systems Group.
†Professor, Defence Academy of the United Kingdom, Head of Aeromechanical Systems Group. Associate Fellow AIAA.
‡Research Student, Defence Academy of the United Kingdom, Aeromechanical Systems Group.

Introduction

ROTATING the nozzles on the propulsion system of a short takeoff, vertical landing (STOVL) aircraft into a splayed configuration (Fig. 1), and thereby altering the vertical component of thrust, provides a means by which the rate of ascent or descent during vertical flight may be controlled. Such a technique overcomes the inherent lag in the turbomachinery, enabling a more rapid response to control demands, which may be important when operating in close proximity to the ground. Splay may also be used to change the strength of the fountain; splaying the jets away from each other reduces the fountain vertical momentum, whereas splaying them inwards increases it [1]. If the jets are splayed inwards such that they merge before impingement with the ground, then no fountain formation occurs. The ability to schedule splay angle with, for example, aircraft height above the ground, provides the opportunity to trade off the beneficial lift-enhancing properties of the fountain flow against its detrimental hot gas ingestion and acoustic fatigue characteristics.

Whilst there have been numerous experimental studies of the fountain flow generated by parallel impinging jets, far fewer have addressed configurations where the jets are splayed. Notable contributions are included in [2–4], however, even these did not focus to any great extent on the effect of splay, regarding it as supplementary to the main investigation of parallel jets. The studies concluded that, in general, outward splay of the jets reduces fountain peak vertical velocity and turbulence intensity. Conversely, inward splay had the opposite effect; fountain vertical velocity and turbulence intensity was increased. This paper addresses the need for a better understanding of the effect of splaying the jets on fountain behavior.

Aims and Objectives

The continued development of STOVL aircraft, both manned and unmanned, with an increasing reliance on computational design techniques, is dependent upon a better understanding of the aerodynamics of jet-lift aircraft in ground effect. The aim of this work was to describe and quantify the fountain upwash flowfield (generated by a pair of impinging, turbulent, compressible jets) in the plane connecting the nozzle centerlines for a range of geometries and nozzle pressure ratios (NPRs). The objectives of the work were to analyze and quantify the effect of nozzle splay angle on

1) jet impingement;
2) the mean flowfield characteristics;

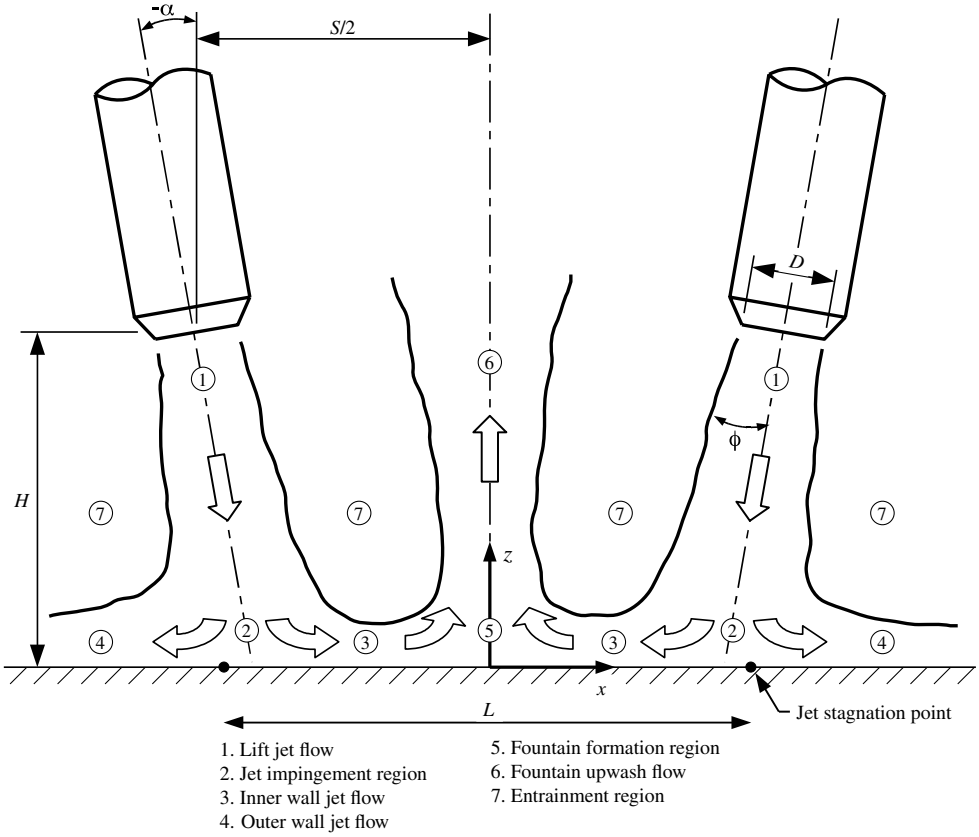

Fig. 1 Schematic of a splayed twin impinging jet fountain flow.

3) the fountain spreading and decay;
4) the fountain momentum flux ratio.

Experimentation

Given that the fountain flow has been shown previously to be highly sensitive to small disturbances caused, for example, by probe interference, this study focused on nonintrusive measurements of the flowfield using particle image velocimetry (PIV).

Impinging Jet Facility

The experiments were conducted in a dedicated impinging jet facility. The test rig (Fig. 2) consisted of a small cylindrical settling chamber with an internal diameter of 230 mm and a height of 210 mm suspended from a $4 \times 4 \times 3$ m^3 steel frame. This rig was mounted in the center of a closed room measuring approximately $8 \times 8 \times 4$ m^3. The settling chamber has two internal screens, and on the lower surface it has a replaceable nozzle-mounting plate that allows different configurations of nozzle spacing and splay angle (Fig. 3). Dried, ambient-temperature compressed air was supplied to the settling chamber through a 63.5 mm diameter flexible hose from two Howden screw-type compressors via a 34 m^3 storage tank. Maximum continuous flow rate was 0.9 kgs^{-1} and maximum pressure was 7 bar(g). The impingement surface consisted of a 1×1 m^2 aluminum plate placed on top of a 3×2 m^2 table. The stagnation pressure in the settling chamber was determined from measurements made, using a Druck PDCR 10-3.5 pressure transducer, of the average of four static pressure tappings equi-spaced around the periphery of the settling chamber (Fig. 2). The error introduced by measuring static pressure rather than stagnation pressure was determined to be negligible due to the very low flow

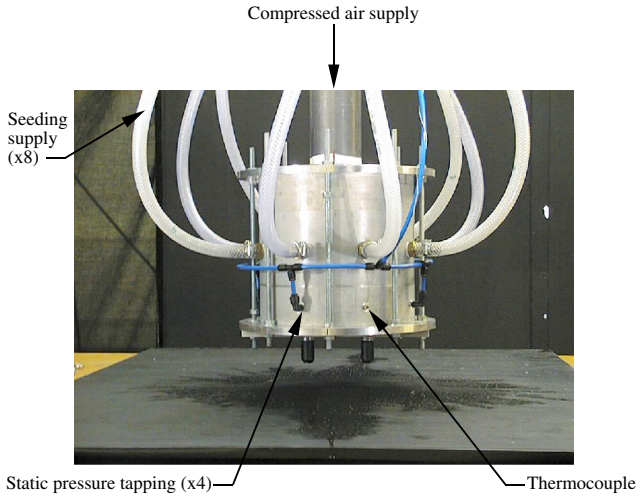

Fig. 2 The settling chamber and impingement surface.

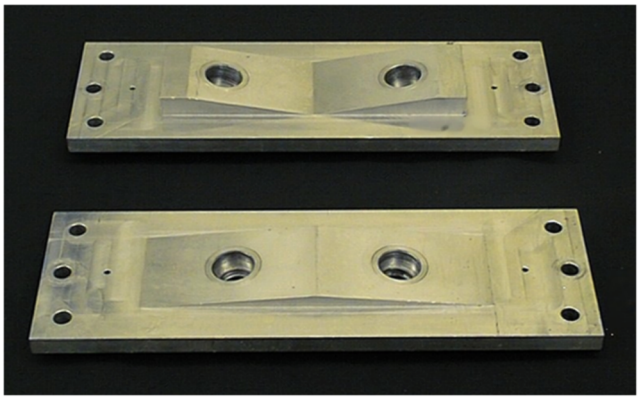

Fig. 3 Splayed nozzle plates: negative (inward) splay, top; positive (outward) splay, bottom.

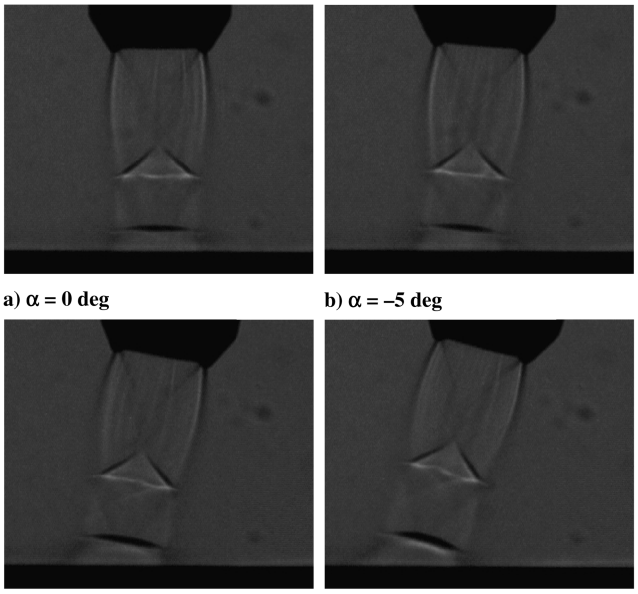

Fig. 4 Shadowgraph images showing impingement of the right-hand jet for four different nozzle splay angles ($H/D = 2.4$, NPR = 3.5).

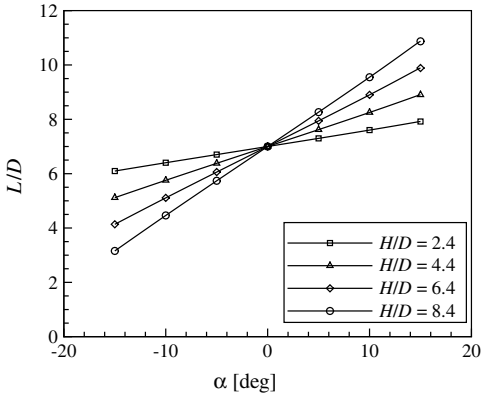

Fig. 6 Theoretical distance between the stagnation points of the jets at impingement.

velocity through the settling chamber [5]. The pressure in the settling chamber was adjusted using a CompAir A119 pneumatically-controlled valve driven by a computer and a current-to-pressure converter. Stagnation temperature in the settling chamber was measured with a *K*-type thermocouple. Atmospheric pressure was measured using a SETRA 270 pressure transducer. The configuration used for this study comprised two identical 63.5 mm long axisymmetric convergent nozzles with an exit diameter, D, of 12.7 mm (following the "short half-inch" nozzle design used by Bray [6]) and a nozzle spacing, S, of seven diameters. The jets were seeded by JEM Hydrosonic long-lasting fluid droplets ($\approx$1 μm diam) generated by a TSI 9306 Six-Jet atomizer connected to a Clarke compressor and injected through eight ports in the settling chamber (Fig. 2). The ambient air was seeded with smoke particles produced by a Le Maitre Turbo Mist fog generator. The uncertainty in the pressure control system was estimated to be $\pm$0.5% of NPR [5].

Particle Image Velocimetry

The PIV equipment consisted of a New Wave Gemini II Nd:YAG double pulsed laser, which through the use of a combination of plano-concave and plano-cylindrical lenses, created a light sheet approximately 1 mm thick, positioned perpendicular to the impingement plane and passing through the plane defined by the nozzle axes. The PIV double pulsed image pairs were acquired using a Kodak Megaplus ES1.0 digital camera with a resolution of 1016 $\times$

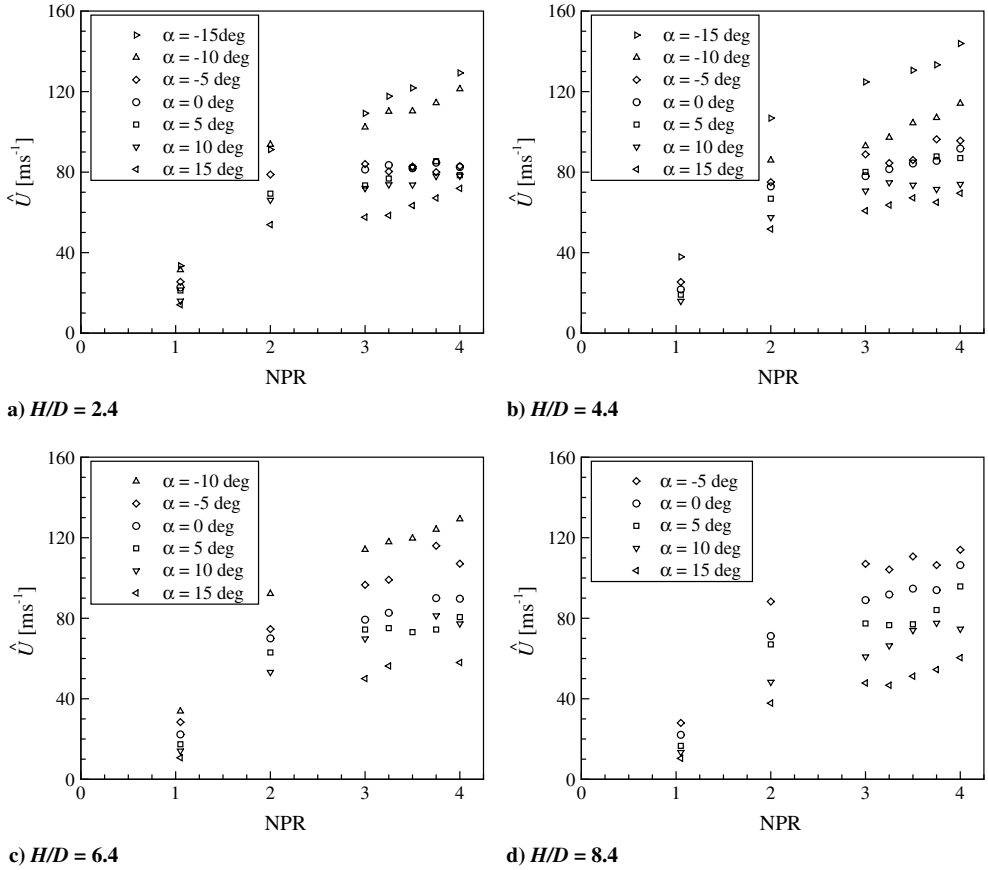

Fig. 5 PIV measured mean peak vertical velocity, $\hat{U}$, in the fountain for a range of nozzle heights, splay angles, and pressure ratios ($S/D = 7$).

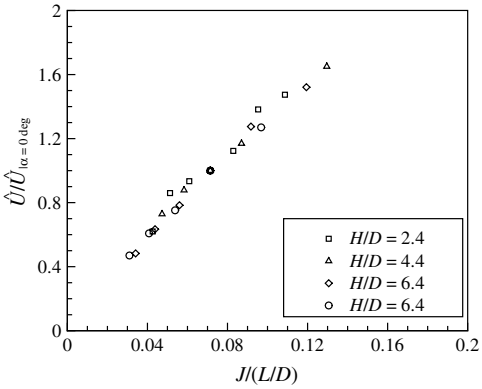

Fig. 7 Nondimensional peak fountain vertical velocity as a function of $J/(L/D)$ ($S/D = 7$, NPR = 1.05).

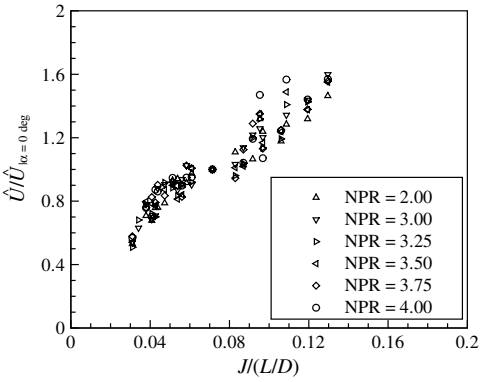

Fig. 8 Nondimensional peak fountain vertical velocity as a function of $J/(L/D)$ for various NPRs ($S/D = 7$, $H/D = 2.4$, 4.4, 6.4 and 8.4).

1008 pixels at a rate of 15 image pairs per second. The camera was fitted with a 60 mm, f2.8 Nikon lens and placed normal to the light sheet at a distance of approximately 550 mm. This provided a maximum field of view of 82×83 mm^2 ($6.4D \times 6.5D$). It was assumed that the maximum velocity in the upwash fountain was around half the maximum jet velocity (assuming isentropic conditions), and the maximum out-of-plane velocity was 25% of the fountain upwash velocity. This resulted in a pulse separation of between 2.6 μs (NPR = 4) and 6.6 μs (NPR = 1.05).

Approximately 500 PIV image pairs were acquired per test case. Data from each image pair consisted of instantaneous streamwise, u, and cross-stream, v, velocities in the z and x directions, respectively. The commercial software Insight v3.3 by TSI was used to process the images. A fast Fourier transform cross-correlation algorithm was used to extract the velocity vectors. Interrogation windows of 32×32 pixels with 75% overlapping were employed in the processing. The size of the interrogation window was chosen to allow for a minimum of ten seeding particles per interrogation area and to allow for the maximum in-plane particle displacement to be less than one quarter of the size of the interrogation window. Inherent to PIV processing are the spurious vectors, which on average, accounted for less than 3% of the total. Images that generated velocity vector fields with spurious vectors of more than 3 standard deviations from the data set mean were rejected (approximately 5%). For those velocity vector fields that were not rejected, spurious vectors were filtered using a bandpass filter followed by a local median filter. The resulting empty spaces were filled with interpolated values from the surrounding area. The uncertainty in the measured velocity using PIV was estimated to be $\pm 3\%$ [5].

Results

Results are presented for PIV measurements made under the following conditions.

1) A nozzle spacing-to-diameter ratio, S/D, of seven.

2) Nozzle height-to-diameter ratios, H/D, of 2.4, 4.4, 6.4, and 8.4.

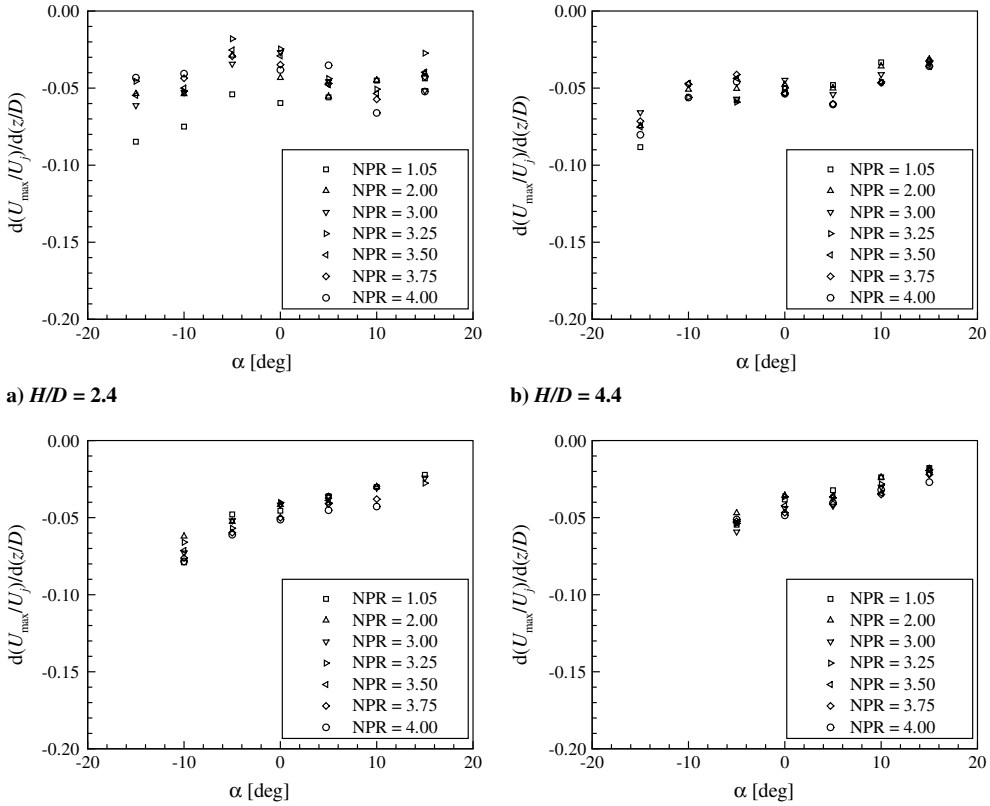

a) H/D = 2.4 **b) H/D = 4.4**

c) H/D = 6.4 **d) H/D = 8.4**

Fig. 9 PIV derived mean fountain vertical velocity decay rate ($S/D = 7$).

3) NPRs of 1.05, 2, 3, 3.25, 3.5, 3.75, and 4.
4) Nozzle splay angles, α, of -15, -10, -5, 0, 5, 10, and 15 deg.

Jet Impingement Region

When the nozzles are splayed, inwards or outwards, two distinct jet flow regions are formed, which are separated by the standoff shock. Upstream of the standoff shock the flow is axisymmetric and resembles that produced by a jet impinging normal to a plane surface; the standoff shock remains parallel with the nozzle exit plane (Fig. 4). Downstream of the standoff shock a nonaxisymmetric flow region is identified. This result is similar to that obtained by a single jet impinging on an inclined surface (see for example the work of Lamont and Hunt [7]) with the exception that the fountain facing part of the jet shear layer is thickened by the fountain's presence [8].

Mean Flowfield

The fountain has been shown to be very sensitive to small variations in the generating jets, ground plane angle and even in the environment surrounding the experimental facilities [3]. Throughout the experiments the jets were generated by the same pair of nozzles, the ground plane was unvarying and the surrounding environment was similar. It was important, therefore, to check that the two jets had as near identical characteristics as possible. Within the limits of experimental uncertainty this was deemed to be the case and Saddington et al. [9] discuss these observations in more detail.

It is already known that splaying the jets away from each other reduces the fountain vertical momentum, whereas splaying them inwards increases it [1]. What is not well understood is how this, and other fountain characteristics, vary with changes in operating parameters such as NPR, height, and splay angle. This is discussed in the following sections for three fountain characteristics: velocity decay, spreading rate, and momentum flux ratio.

Velocity Decay

The effect of nozzle height, splay, and pressure ratio on the time–mean peak vertical velocity in the fountain, $\hat{U}$, is shown in Fig. 5.

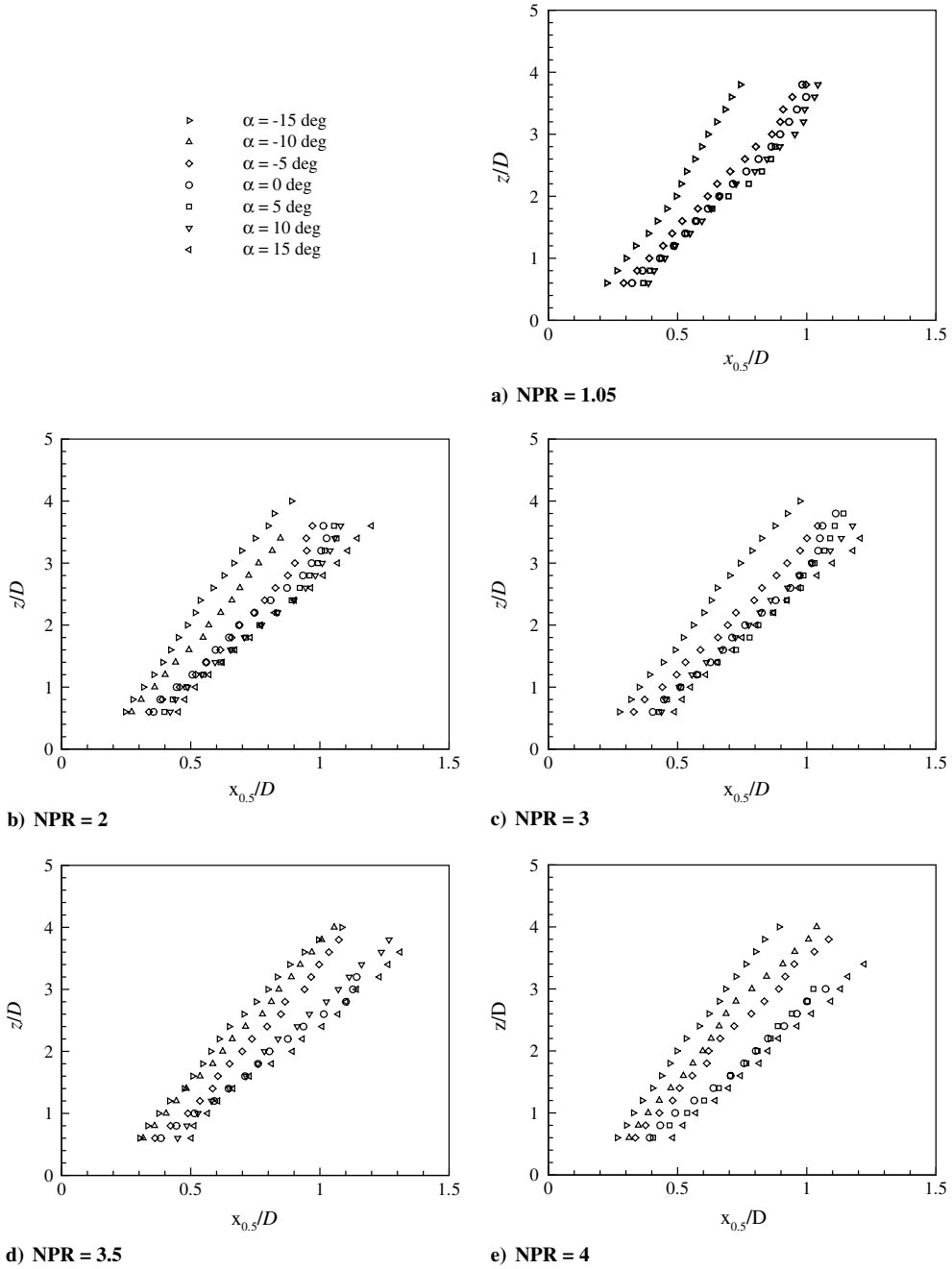

Fig. 10 PIV derived variation of fountain half-width, $x_{0.5}/D$, with distance above the ground plane, z/D ($H/D = 4.4$, $S/D = 7$).

($\hat{U}$ is the highest measured vertical velocity in the fountain, whereas $U_{\max}$ is the highest measured vertical velocity in the fountain at a specific height.) For a fixed nozzle height, peak vertical velocity in the fountain was observed to be highly dependent upon the splay angle, with NPR having a secondary influence under choked nozzle conditions. Between NPR = 1.05 and NPR = 2, however, an increased upwash velocity was evident. The variation of peak fountain upwash velocity with NPR showed a strong dependence upon splay angle and a lesser dependence upon nozzle height. Increasing NPR for configurations with $\alpha = -15$ and -10 deg resulted in the largest increase of peak vertical velocity. For a given NPR the largest peak upwash velocity was obtained with $\alpha = -15$ deg and $H/D = 4.4$.

To further investigate the effect of parametric changes on the peak upwash velocity a method was sought by which the data could be nondimensionalized. The ratio of peak vertical velocity in the fountain with a given nozzle height and splay angle to peak vertical velocity at the same nozzle height but with zero splay angle,

$$\frac{\hat{U}}{\hat{U}_{|\alpha=0 \text{ deg}}} \tag{1}$$

was used to nondimensionalize the velocity magnitude.

As nozzle splay angle is reduced the jets impinge closer to the geometric center of the fountain; for certain configurations the jets may merge before impingement. This was observed to occur for the following configurations: $H/D = 6.4$, $\alpha = -15$ deg; $H/D = 8.4$, $\alpha = -15$ deg; $H/D = 8.4, \alpha = -10$ deg. Schach [10] showed that at impingement the stagnation point of an inviscid, incompressible, inclined jet is shifted $(D/2)\tan\alpha$ along the impingement plane towards the origin of inclination, that is, for the situation shown in Fig. 1 the stagnation point will be to the left of the extended centerline of the left-hand jet and to the right of the extended centerline of the right-hand jet.

For viscous conditions the change in nondimensional distance between the stagnation points associated with the two jets is a function of the spreading rate of the jets as well as the nozzle height, spacing, and splay angle. Following Bray's analysis of his own experimental data [6] the jets have been assumed to have a half-angle, ϕ, of 4.6 deg. The work of Schach [10] has, therefore, been extended here to include the effect of jet spreading, and with reference to the geometric characteristics shown in Fig. 1, Eq. (2) was derived.

$$\frac{L}{D} = \frac{S}{D} + \frac{2H\tan\alpha}{D} - \left[\left\{\frac{2H\tan\alpha}{D} + \cos\alpha\right\} - \left\{\left(\frac{2H}{D} - \sin\alpha\right)\tan(\alpha - \phi)\right\}\right]\sin\alpha \tag{2}$$

where α is the splay angle and ϕ is the jet spreading half-angle. Eq. (2) is presented in graphical form in Fig. 6. When $\phi = 0$ deg the third term in Eq. (2) simplifies to $\tan\alpha$, which is Schach's result in nondimensional terms.

As well as affecting jet separation at impingement, nozzle splay also affects the proportion of total jet momentum flowing downstream away from the origin of the nozzle inclination (inwards towards the fountain in Fig. 1). Schach [10] gives the following equation for this ratio, based on an inviscid analysis:

$$J = 1 - \frac{\pi/2 + \alpha}{\pi} + \frac{\sin(2(\pi/2 + \alpha))}{2\pi} \tag{3}$$

Rubel [11] has shown Eq. (3) to be in good agreement with the experimental measurements of viscous jets by Taylor [12]. Figure 7 presents the ratio of nondimensional peak vertical velocity in the fountain, $\hat{U}/\hat{U}_{|\alpha=0 \text{ deg}}$, as a function of $J/(L/D)$ for NPR = 1.05. At such a low pressure ratio the effect of the shock cells observed at higher pressure ratios can be eliminated. The figure shows that, for the range of nozzle heights and splay angles considered, the data collapses quite well onto a single trend. A negative (inward) splay of

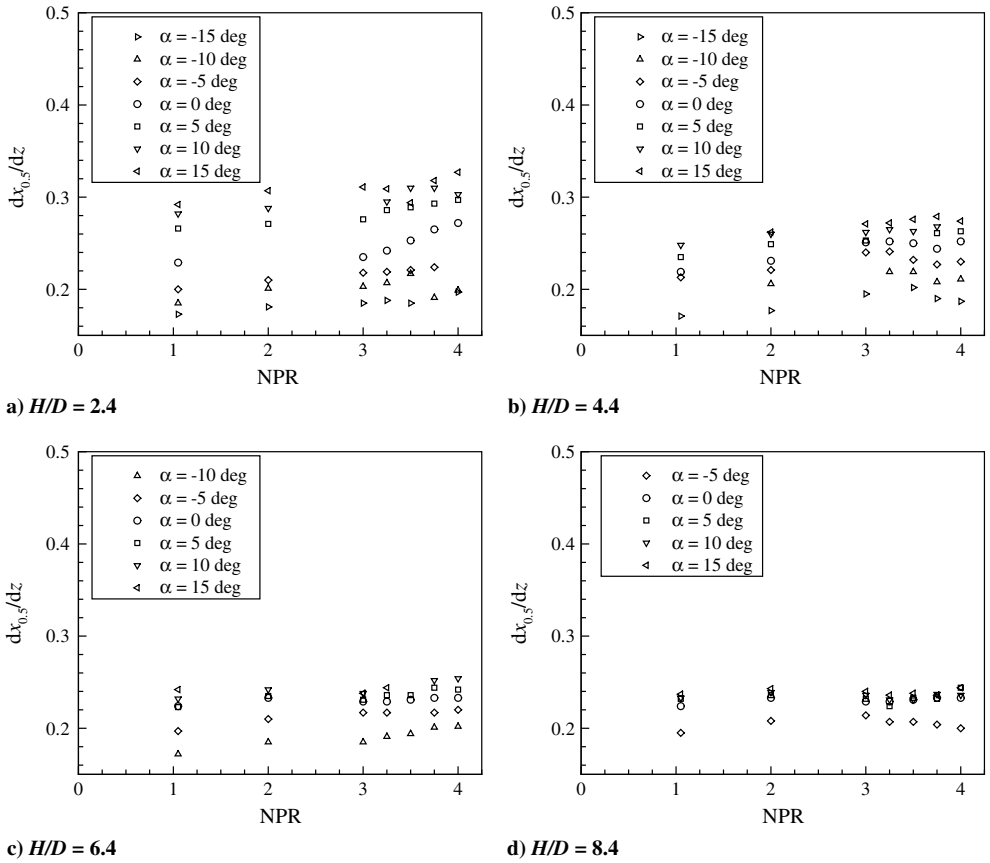

Fig. 11 PIV derived growth rate of the fountain half-width, $dx_{0.5}/dz$ ($S/D = 7$).

the nozzles increases the nondimensional peak fountain vertical velocity; decreasing the distance between the jets at impingement has the same effect.

Considering the configurations with underexpanded nozzle conditions the situation is not quite so straightforward. In general, the trend is similar to that presented in Fig. 7, however, there is significantly more scatter in the data in Fig. 8 that we attribute to shock-dependent effects. The strength of the standoff shock is influenced by the underexpanded flow upstream of impingement (shock-cell structure). This underexpanded flow field is determined by the values of NPR [13] and the height of the nozzle above the ground, but in a complex and interdependent manner. The peak vertical velocity in the fountain appears, therefore, to be quite sensitive to the point within the shock cell at which impingement occurs. It is observed that there is a wider scatter for negative splay than for positive splay and it is suggested here that this may be associated with increased fountain instability in the former case [5].

Figure 9 shows the rate of decay of maximum vertical velocity in the fountain, $\mathrm{d}(U_{\max}/U_j)/\mathrm{d}(z/D)$. For a nondimensional nozzle height, H/D, of 2.4 (Fig. 9a), the data shows that the decay rate has a strong dependence upon NPR and the variation in the decay rate with nozzle splay angle is nonlinear. There is a general trend, however, indicating that the rate of mean fountain vertical velocity decay decreases with increasing nozzle splay angle.

The NPR dependence is much reduced when the nozzle height is increased to $H/D = 4.4$ (Fig. 9b), however, the nonlinear variation of decay rate with nozzle splay angle remains. Increasing nozzle height further to $H/D = 6.4$ (Fig. 9c) and $H/D = 8.4$ (Fig. 9d) reveals a much more linear variation of mean fountain vertical velocity decay rate with nozzle splay angle. There is still some scatter of the data in relation to NPR changes but this is not significant.

Spreading Rate

Values of fountain half-width, $x_{0.5}$, were extracted from the mean velocity data for all nozzle configurations. The half-width was only calculated where the condition $U/U_{\max} < 0.5$ was satisfied on both sides of the fountain velocity profile. An example of the variation of

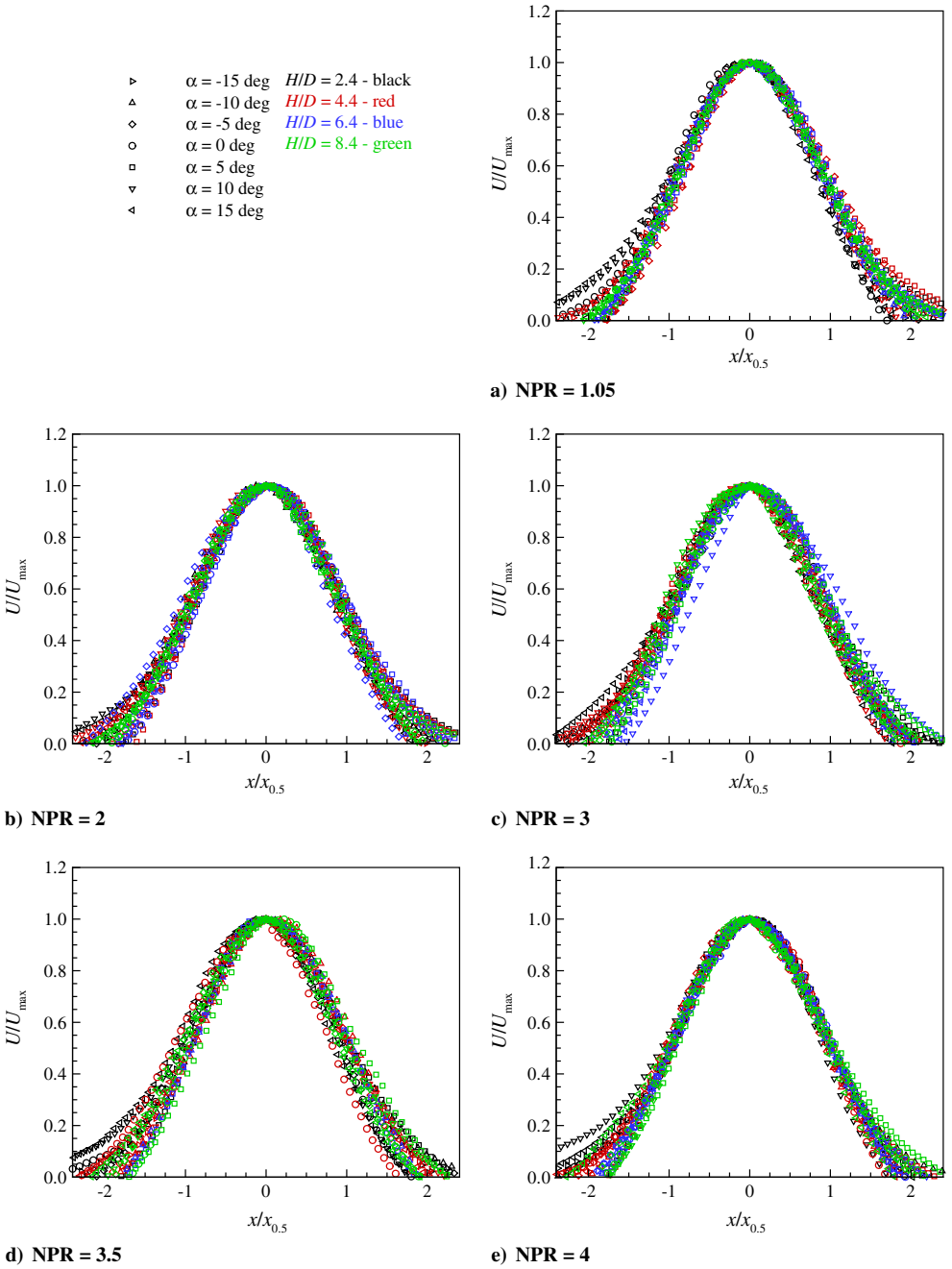

Fig. 12 PIV measured nondimensional mean vertical velocity profiles ($S/D = 7, z/D = 1.5$).

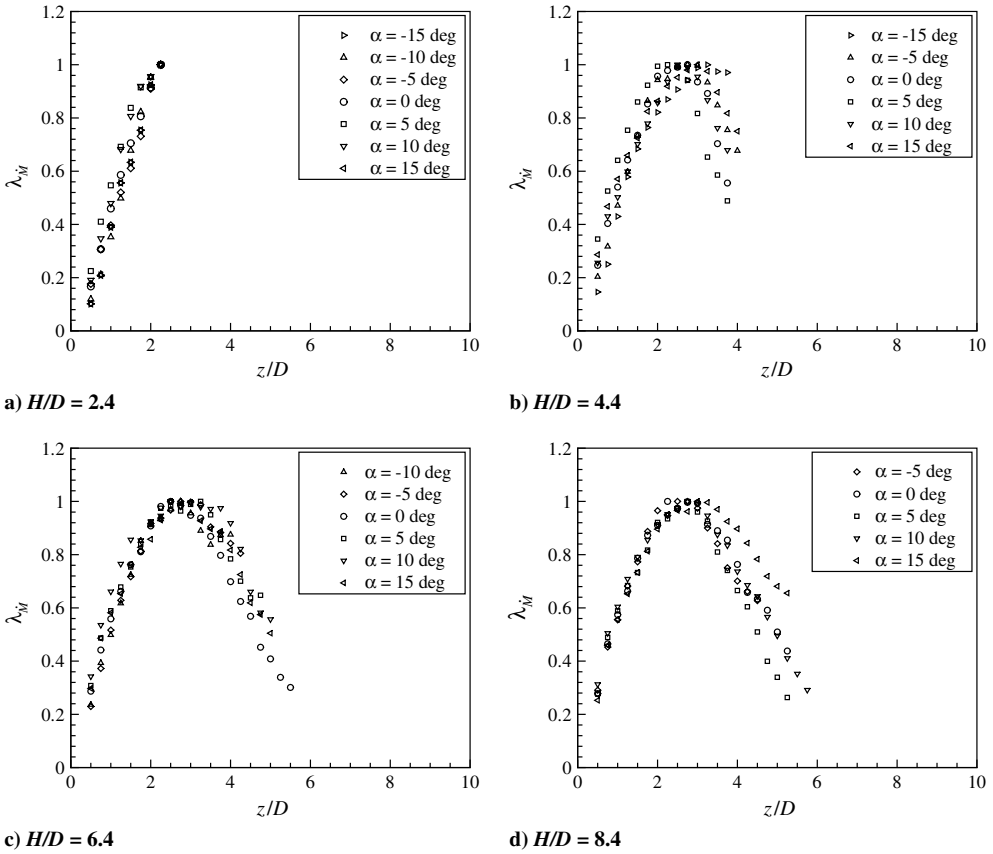

Fig. 13 PIV derived vertical distribution of momentum flux ratio, $\lambda_{\dot{M}}$, through the fountain (NPR = 3, $S/D = 7$).

fountain half-width with distance above the ground is shown in Fig. 10 for $H/D = 4.4$. Fountain half-width was found to vary quite linearly with height above the ground for all the tested conditions. Negative (inward) splayed nozzle configurations presented the smallest values of fountain half-width, demonstrating that the fountain becomes narrower with decreasing splay angle. This qualitative variation of fountain half-width with splay angle was consistently observed for each combination of nozzle height and pressure ratio.

The fountain's growth rate (or spreading rate), the variation of $x_{0.5}$ with distance from the impingement plane, can be represented by

$$\frac{x_{0.5}}{D} = a_1\left(\frac{z}{D}\right) + a_2 \tag{4}$$

where a_1 is the growth rate of the fountain half-width, and a_2 is the half-width at $z = 0$: a_2 can also be written in terms of a fountain virtual origin, z_0, (the value of z at $x_{0.5} = 0$) as $a_2 = -a_1 z_0/D$. Although at the fountain base the half-width is approximately constant for a given splay angle, its variation with increasing height above the ground, defined by the growth rate, $\mathrm{d}x_{0.5}/\mathrm{d}z$, is quantitatively different across the test matrix as shown in Fig. 11.

Nozzle splay angle has the greatest influence on fountain growth rate compared with NPR. It is evident that with a low nozzle height, varying nozzle splay angle and NPR induces larger variations in the fountain growth rate than at high nozzle heights. At $H/D = 2.4$ the average variation in spreading rate (relative to the parallel nozzle configuration) with splay angle was 70%; the average variation with NPR was 15%. At $H/D = 8.4$ these values reduce to 15% and 5%, respectively. The effect of changing nozzle splay angle is noticeably different at different nozzle heights. With increasing nozzle height, increasing nozzle splay angle (for $\alpha > 0$ deg) produces a smaller increase in the fountain growth rate. For example, on average, increasing nozzle splay angle from $\alpha = 0$ deg to $\alpha = 15$ deg results in a 25% increase in the fountain growth rate at $H/D = 2.4$. The same variation in splay angle at $H/D = 8.4$ only results in a 5% increase in fountain growth rate.

Momentum Flux Ratio

In [9] it was shown that vertical velocity profiles, when nondimensionalized with the local maximum mean fountain upwash velocity, $U_{\max}$, and fountain half-width, $x_{0.5}$, were self-similar for all nozzle heights and pressure ratios under investigation. In this study, with splayed nozzle configurations, profiles of mean vertical velocity were also found to exhibit self-similarity and this behavior occurred independently of nozzle height, splay angle, and pressure ratio. An example is shown in Fig. 12 for $z/D = 1.5$.

Momentum flux ratio was calculated using the same method as that described in [9]. Generally, it was found that the inclusion of nozzle splay did not significantly alter the distribution of fountain momentum flux ratio, $\lambda_{\dot{M}}$, relative to the equivalent parallel configuration. At a nozzle height of $H/D = 4.4$ the position of maximum momentum flux ratio occurred further downstream in the fountain (at a higher value of z/D) for configurations with negative nozzle splay angles (Fig. 13). For configurations with negative nozzle splay angles the position of maximum momentum flux ratio occurred at $z/D \approx 3.25$, whereas for configurations with parallel and positive nozzle splay angles the position of maximum momentum flux ratio was found to occur at $z/D \approx 2.5$.

At $H/D = 6.4$ and $H/D = 8.4$ there is a strong similarity between the distributions of momentum flux ratio across the range of nozzle splay angles and pressure ratios; Fig. 13 shows the case for NPR = 3. In general, the position of maximum momentum flux ratio occurred at $z/D \approx 2.8$ ($H/D = 6.4$) and $z/D \approx 3.0$ ($H/D = 8.4$).

Conclusions

An investigation has been conducted on the fountain flowfield formed by the impingement of two high-speed, turbulent, compressible jets. Mean fountain characteristics were acquired for NPRs

of between 1.05 and 4, nozzle height-to-diameter ratios of between 2.4 and 8.4, nozzle splay angles of between ± 15 deg and a nozzle spacing-to-diameter ratio of seven. Shadowgraph images of the jet impingement region showed that the standoff shock remains parallel to the nozzle exit plane even when the jet is inclined to the impingement plane by up to 15 deg. It was shown that for a low NPR (1.05) there was good correlation between, the product of the jet momentum carried towards the fountain formation region and the lateral separation of the jet stagnation points, and the ratio of peak vertical velocity in the fountain. For underexpanded pressure ratios the correlation still exists, however, there was more scatter in the data. This was thought to be due to changes in the shock-cell structure caused, for example, by small changes in NPR having a strong influence on the jet velocity at impingement. The rate of decay of maximum vertical velocity in the fountain was shown to have a strong dependence on NPR and the variation in decay rate with nozzle splay angle is, at the lower nozzle heights, nonlinear with nozzle splay angle. Fountain spreading rate was observed to have a strong dependence upon nozzle splay angle at low nozzle heights but a negligible dependence once nozzle height had reached 8.4 diam. In general, it was found that the inclusion of nozzle splay did not significantly alter the distribution of fountain momentum flux ratio relative to the equivalent parallel configuration.

Acknowledgement

This work was partly funded by the Engineering and Physical Sciences Research Council under grant GR/R42894/01 and their support is gratefully acknowledged.

References

[1] Kuhn, R. E., Margason, R. J., and Curtis, P., *Jet Induced Effects: The Aerodynamics of Jet and Fan Powered V/STOL Aircraft in Hover and Transition*, Progress in Astronautics and Aeronautics, Vol. 217, AIAA, Reston, VA, 2006.

[2] Kibens, V., Saripalli, K. R., Wlezien, R. W., and Kegelman, J. T., "Unsteady Features of Jets in Lift and Cruise Modes for VTOL Aircraft," *International Powered Lift Conference and Exhibit*, SAE, Paper 872359, 7–10 Dec. 1987, pp. 543–552.

[3] Abbott, W. A., and White, D. R., "The Effect of Nozzle Pressure Ratio on the Fountain Formed Between Two Impinging Jets," Technical Memorandum P1166, Royal Aircraft Establishment, 1989.

[4] Behrouzi, P., and McGuirk, J. J., "Experimental Data for CFD Validation of Impinging Jets in Cross-flow with Application to ASTOVL Flow Problems," *Fluid Dynamics Panel Symposium*, CP-534, AGARD, 19–22 April 1993.

[5] Cabrita, P. M., "Steady and Unsteady Features of Twin-Jet STOVL Ground Effects," Ph.D. thesis, Cranfield University, Shrivenham, UK, 2006.

[6] Bray, D., *Jets in Cross-flow and Ground Effect*, Ph.D. thesis, Cranfield Institute of Technology, Shrivenham, UK, 1992.

[7] Lamont, P. J., and Hunt, B. L., "The Impingement of Underexpanded, Axisymmetric Jets on Perpendicular and Inclined Flat Plates," *Journal of Fluid Mechanics*, Vol. 100, No. 3, 1980, pp. 471–511. doi:10.1017/S0022112080001255

[8] Cabrita, P. M., Saddington, A. J., and Knowles, K., "PIV Study of a Twin-jet STOVL Fountain Flow," *The Aeronautical Journal*, Vol. 109, No. 1100, Oct. 2005, pp. 439–449.

[9] Saddington, A. J., Knowles, K., and Cabrita, P. M., "Flow Measurements in a Short Take-Off, Vertical Landing Fountain: Parallel Jets," *Journal of Aircraft*, Vol. 45, No. 5, 2008, pp. 1736–1743. doi:10.2514/1.32599

[10] Schach, W., "Umlenkungeinesfreien Flussigkeitsstrahles an einer ebenen Platte," *Ingenieur-Archiv*, Vol. 5, No. 4, Aug. 1934, pp. 245–265; also *The Deflection of a Free Liquid Jet on a Flat Plane* (in English). doi:10.1007/BF02084152

[11] Rubel, A., "Oblique Impingement of a Round Jet on a Plane Surface," *AIAA Journal*, Vol. 20, No. 12, 1982, pp. 1756–1758. doi:10.2514/3.8016

[12] Taylor, G., "Formation of Thin Flat Sheets of Water," Proceedings of the Royal Society of London, *Series A, Mathematical and Physical Sciences*, Vol. 259, No. 1296, Nov. 1960, pp. 1–17.

[13] Saddington, A. J., Lawson, N. J., and Knowles, K., "An Experimental and Numerical Investigation of Under-Expanded Turbulent Jets," *The Aeronautical Journal*, Vol. 108, No. 1081, 2004, pp. 145–152.